Towards an analytical framework for tailoring supercontinuum generation

DAVID CASTELLÓ-LURBE,[1,*] NATHALIE VERMEULEN,[1] AND ENRIQUE SILVESTRE[2]

[1]*Brussels Photonics Team (B-PHOT), Department of Applied Physics and Photonics (IR-TONA), Vrije Universiteit Brussel, Pleinlaan 2, B-1050 Brussels, Belgium*

[2]*Departament d'Òptica, Universitat de València, E-46100 Burjassot, Spain*

[*]*david.castello-lurbe@vub.ac.be*

Abstract: A fully analytical toolbox for supercontinuum generation relying on scenarios without pulse splitting is presented. Furthermore, starting from the new insights provided by this formalism about the physical nature of direct and cascaded dispersive wave emission, a unified description of this radiation in both normal and anomalous dispersion regimes is derived. Previously unidentified physics of broadband spectra reported in earlier works is successfully explained on this basis. Finally, a foundry-compatible few-millimeters-long silicon waveguide allowing octave-spanning supercontinuum generation pumped at telecom wavelengths in the normal dispersion regime is designed, hence showcasing the potential of this new analytical approach.

OCIS codes: (130.3120) Integrated optics devices, (190.4390) Nonlinear optics, integrated optics.

References and links

1. J. M. Dudley, G. Genty, and S. Coen, "Supercontinuum generation in photonic crystal fiber," Rev. Mod. Phys. **78**, 1135–1184 (2006).
2. D. V. Skryabin and A. V. Gorbach, "Looking at a soliton through the prism of optical supercontinuum," Rev. Mod. Phys. **82**, 1287–1299 (2010).
3. M. Conforti and S. Trillo, "Dispersive wave emission from wave breaking," Opt. Lett. **38**, 3815–3818 (2013).
4. D. V. Skryabin and A. V. Yulin, "Theory of generation of new frequencies by mixing of solitons and dispersive waves in optical fibers," Phys. Rev. E **72**, 016619 (2005).
5. A. V. Gorbach, D. V. Skryabin, J. M. Stone, J. C. Knight, "Four-wave mixing of solitons with radiation and quasi-nondispersive wave packets at the short-wavelength edge of a supercontinuum," Opt. Express **14**, 9854–9863 (2006).
6. A. V. Gorbach, D. V. Skryabin, "Light trapping in gravity-like potentials and expansion of supercontinuum spectra in photonic-crystal fibres," Nature Photon. **1**, 653–657 (2007).
7. Y. R. Shen, *The Principles of Nonlinear Optics* (John Wiley & Sons, 2003).
8. A. Ferrando, M. Zacarés, P. Fernández de Córdoba, D. Binosi, and Á. Montero, "Forward-backward equations for nonlinear propagation in axially invariant optical systems," Phys. Rev. E **71**, 016601 (2005).
9. M. Kolesik, E. M. Wright, J. V. Moloney, "Simulation of femtosecond pulse propagation in sub-micron diameter tapered fibers," Appl. Phys. B **79**, 293–300 (2004).
10. B. A. Daniel and G. P. Agrawal, "Vectorial nonlinear propagation in silicon nanowire waveguides: polarization effects," J. Opt. Soc. Am. B **27**, 956–965 (2010).
11. Sh. Amiranashvili and A. Demircan, "Ultrashort optical pulse propagation in terms of analytic signal," Adv. Opt. Technol. **2011**, 989515 (2011).
12. P. K. A. Wai, C. R. Menyuk, Y. C. Lee, and H. H. Chen, "Nonlinear pulse propagation in the neighborhood of the zero-dispersion wavelength of monomode optical fibers," Opt. Lett. **11**, 464–466 (1986).
13. N. Akhmediev and M. Karlsson, "Cherenkov radiation emitted by solitons in optical fibers," Phys. Rev. A **51**, 2602–2607 (1995).
14. A. V. Husakou and J. Herrmann, "Supercontinuum generation of higher-order solitons by fission in photonic crystal fibers," Phys. Rev. Lett. **27**, 203901 (2001).
15. I. Cristiani, R. Tediosi, L. Tartara and V. Degiorgio, "Dispersive wave generation by solitons in microstructured optical fibers," Opt. Express **12**, 124–135 (2004).
16. G. Chang, L. Chen, and F. X. Kärtner, "Highly efficient Cherenkov radiation in photonic crystal fibers for broadband visible wavelength generation," Opt. Lett. **35**, 2361–2363 (2010).
17. X. Liu, J. Læsgaard, U. Møller, H. Tu, S. A. Boppart, and D. Turchinovich, "All-fiber femtosecond Cherenkov radiation source," Opt. Lett. **37** 2769–2771 (2012).

18. Y. Kodama and A. Hasegawa, "Nonlinear pulse propagation in a monomode dielectric guide," IEEE J. Quantum Electron. **23**, 510–524 (1987).
19. D. R. Austin, C. M. de Sterke, B. J. Eggleton, and T. G. Brown, "Dispersive wave blue-shift in supercontinuum generation," Opt. Express **14**, 11997–12007 (2006).
20. L. Zhang, Q. Lin, Y. Yue, Y. Yan, R. G. Beausoleil, and A. E. Willner, "Silicon waveguide with four zero-dispersion wavelengths and its application in on-chip octave-spanning supercontinuum generation," Opt. Express **20**, 1685–1690 (2012).
21. A. R. Johnson, A. S. Mayer, A. Klenner, K. Luke, E. S. Lamb, M. R. E. Lamont, C. Joshi, Y. Okawachi, F. W. Wise, M. Lipson, U. Keller, and A. L. Gaeta, "Octave-spanning coherent supercontinuum generation in a silicon nitride waveguide," Opt. Lett. **40**, 5117–5120 (2015).
22. K. E. Webb, Y. Q. Xu, M. Erkintalo, and S. G. Murdoch, "Generalized dispersive wave emission in nonlinear fibers," Opt. Lett. **38**, 151–153 (2013).
23. D. Castelló-Lurbe and E. Silvestre, "Supercontinuum generation in silicon waveguides relying on wave-breaking," Opt. Express **23**, 25462–25473 (2015).
24. X. Fang, N. Karasawa, R. Morita, R. S. Windeler, and M. Yamashita, "Nonlinear propagation of a-few-optical-cycle pulses in a photonic crystal fiber — Experimental and theoretical studies beyond the slowly varying-envelope approximation," IEEE Photon. Technol. Lett. **15**, 233–235 (2003).
25. S. Coen, A. H. L. Chau, R. Leonhardt, J. D. Harvey, J. C. Knight, W. J. Wadsworth, and P. St. J. Russell, "White-light supercontinuum generation with 60-ps pump pulses in a photonic crystal fiber," Opt. Lett. **26**, 1356–1358 (2001).
26. G. Genty, M. Lehtonen, H. Ludvigsen, J. Broeng, and M. Kaivola, "Spectral broadening of femtosecond pulses into continuum radiation in microstructured fibers," Opt. Express **10**, 1083–1098 (2002).
27. M. Erkintalo, Y. Q. Xu, S. G. Murdoch, J. M. Dudley, and G. Genty, "Cascaded phase matching and nonlinear symmetry breaking in fiber frequency combs," Phys. Rev. Lett. **109**, 223904 (2012).
28. K. E. Webb, M. Erkintalo, Y. XU, N. G. R. Broderick, J. M. Dudley, G. Genty, and S. G. Murdoch, "Nonlinear optics of fibre event horizons," Nat. Commun. 5:4969 doi: 10.1038/ncomms5969 (2014).
29. Y. Q. Xu, M. Erkintalo, G. Genty, and S. G. Murdoch, "Cascaded Bragg scattering in fiber optics," Opt. Lett. **38**, 142–144 (2013).
30. W. J. Tomlinson, R. H. Stolen, and A. M. Johnson, "Optical wave-breaking in nonlinear optical fibers," Opt. Lett. **10**, 457-459 (1985).
31. D. Anderson, M. Desaix, M. Lisak, and M. L. Quiroga-Teixeiro, "Wave breaking in nonlinear-optical fibers," J. Opt. Soc. Am. B **9**, 1358–1361 (1992).
32. M. Conforti, F. Baronio, and S. Trillo, "Resonant radiation shed by dispersive shock waves," Phys. Rev. A **89**, 013807 (2014).
33. G. A. Nowak, J. Kim, and M. N. Islam, "Stable supercontinuum generation in short lengths of conventional dispersion-shifted fiber," Appl. Opt. **38**, 7364–7369 (1999).
34. C. Chen and P. L. Kelley, "Nonlinear pulse compression in optical fibers: scaling laws and numerical analysis," J. Opt. Soc. Am. B **19**, 1961–1967 (2002).
35. N. Vermeulen, J. Cheng, J. E. Sipe, and H. Thienpont, "Opportunities for wideband wavelength conversion in foundry-compatible silicon waveguides covered with graphene," IEEE J. Sel. Top. Quantum Electron. **22**, 8100113 (2016).
36. D. Castelló-Lurbe, P. Andrés, and E. Silvestre, "Dispersion-to-spectrum mapping in nonlinear fibers based on optical wave-breaking," Opt. Express **21**, 28550–28558 (2013).
37. V. E. Zakharov and A. B. Shabat, "Exact theory of two-dimensional self-focusing and one-dimensional self-modulation of waves in nonlinear media," Sov. Phys. JETP **34**, 62–70 (1972).
38. G. P. Agrawal, *Nonlinear Fiber Optics* (Academic Press, 4th ed., 2007).
39. J. E. Rothenberg and D. Grischkowsky, "Observation of the formation of an optical intensity shock and wave breaking in the nonlinear propagation of pulses in optical fibers," Phys. Rev. Lett. **62**, 531–534 (1989).
40. J. E. Rothenberg, "Femtosecond optical shocks and wave breaking in fiber propagation," J. Opt. Soc. Am. B **6**, 2392–2401 (1989).
41. G. Xu, A. Mussot, A. Kudlinski, S. Trillo, F. Copie, and M. Conforti, "Shock wave generation triggered by a weak background in optical fibers," Opt. Lett. **41**, 2656–2659 (2016).
42. J. M. Dudley, L. P. Barry, P. G. Bollond, J. D. Harvey, R. Leonhardt, and P. D. Drummond, "Direct measurement of pulse distortion near the zero-dispersion wavelength in an optical fiber by frequency-resolved optical gating," Opt. Lett. **22**, 457–459 (1997).
43. F. Leo, S. Gorza, J. Safioui, P. Kockaert, S. Coen, U. Dave, B. Kuyken, and G. Roelkens, "Dispersive wave emission and supercontinuum generation in a silicon wire waveguide pumped around the 1550 nm telecommunication wavelength," Opt. Lett. **39**, 3623–3626 (2014).
44. R. K. W. Lau, M. R. E. Lamont, A. G. Griffith, Y. Okawachi, M. Lipson, and A. L. Gaeta, "Octave-spanning mid-infrared supercontinuum generation in silicon nanowaveguides," Opt. Lett. **39**, 4518–4521 (2014).
45. D. Castelló-Lurbe, V. Torres-Company, and E. Silvestre, "Inverse dispersion engineering in silicon waveguides," J. Opt. Soc. Am. B **31**, 1829–1835 (2014).
46. See ePIXfab at http://www.epixfab.eu and Institute of Microelectronics (IME) at https://www.a-star.edu.sg/.

47. B. Kuyken, X. Liu, R. M. Osgood Jr., R. Baets, G. Roelkens, and W. M. J. Green, "Mid-infrared to telecom-band supercontinuum generation in highly nonlinear silicon-on-insulator wire waveguides," Opt. Express **19**, 20172–20181 (2011).
48. T. Wang, N. Venkatram, J. Gosciniak, Y. Cui, G. Qian, W. Ji, and D. T. H. Tan, "Multi-photon absorption and third-order nonlinearity in silicon at mid-infrared wavelengths," Opt. Express **21**, 32192–32198 (2013).
49. A. D. Bristow, N. Rotenberg, and H. M. van Driel, "Two-photon absorption and Kerr coefficients of silicon for 850–2200 nm," Appl. Phys. Lett. **90**, 191104 (2007).
50. L. Yin, Q. Lin, G. P. Agrawal, "Soliton fission and supercontinuum generation in silicon waveguides," Opt. Lett. **32**, 391–393 (2007).
51. S. Lefrancois, C. Husko, A. Blanco-Redondo, and B. J. Eggleton, "Nonlinear silicon photonics analyzed with the moment method," J. Opt. Soc. Am. B **32**, 218–226 (2015).

1. Introduction

Supercontinuum (SC) generation is a complex nonlinear phenomenon that can rely on different mechanisms leading to a rich phenomenology. It can be described by generalizations of the standard nonlinear Schrödinger equation (NLSE). Particularly, high-order dispersion (HOD) plays a key role for SC generation [1]. Moreover, the theoretical analysis of SC is often challenging because it must address nonlinear pulse evolution away from stationary states such as solitons. As a result, most of the studies look for approximate solutions to the NLSE based on a suitable *ansatz* and different perturbative methods [2, 3]. They give rise to effective theories that are extremely valuable to deal with complex scenarios such as soliton fission and subsequent processes [4–6]. Although such theories are often needed, it cannot be assumed that this fully mathematical approach is always the most convenient.

In nonlinear photonics, the NLSE can be derived from Maxwell's equations when backscattered waves induced by nonlinearities are neglected (this corresponds to the slowly-varying envelope approximation in the z coordinate [7] and converts the second-order wave equation into a first-order equation) [8] and when diffraction is addressed by means of modal methods (this allows separating transverse and longitudinal coordinates and reduces the model to a single equation if monomode propagation can be assumed) [9]. These approximations do not affect the nonlinear processes allowed in the medium [7, 10]. If only the third-order polarization that accounts for $\omega_1 + \omega_2 \rightarrow \omega_3 + \omega_4$, *i.e.*, the four-wave mixing (FWM) process, is retained, then the standard NLSE arises [11]. From this point of view, although new frequency generation can be analyzed based on a mathematical solution of NLSE — a high-level concept —, it necessarily relies on FWM processes — a low-level concept. The level of detail of a description will depend on the nature of the problem itself, but also on the purposes of the description. In scenarios where many FWM processes take place or intricate interplays between dispersion and nonlinearities over the whole pulse are produced (giving rise to, *e.g.*, solitons), low-level descriptions are often not useful. However, if the pulse spectrum develops well-defined resonances through, *e.g.*, dispersive wave (DW) emission, one might ask if the dominant FWM processes could be identified in this case and so, a low-level description could be derived.

DW emission refers to the formation of spectral resonances due to HOD [12]. This mechanism plays a crucial role for SC generation [1, 2, 14, 15] and particularly, it was recently exploited for efficient wavelength conversion into the visible range in photonic crystal fiber (PCF) [16, 17]. It was pointed out early that optical solitons perturbed by HOD [*e.g.*, propagating in the neighborhood of the zero-dispersion frequency (ZDF)] radiated at specific frequencies [12]. An effective radiative process involving the soliton [*i.e.*, a nonlinear wave-packet] and a small-amplitude signal [*i.e.*, a linear, often narrow-band, wave-packet] was considered to analyze this phenomenon [13]. With this approach one succeeded in finding the phase-matching condition that leads to the resonant frequency.

Spectral resonances observed in SC in PCFs and integrated waveguides were usually interpreted as DWs radiated by the solitons emerged after soliton fission [1]. According to [18], a

higher-order soliton is a bound state of fundamental solitons. However, it becomes unstable in the presence of small perturbations [*e.g.*, HOD or stimulated Raman scattering (SRS)] and tends to split into its constituent solitons after propagation. Consequently, the pulse splitting that precedes radiative processes can be analyzed as soliton fission, and the subsequent generation of spectral resonances (also called nonsolitonic radiation) as DWs radiated by the solitons emerged after fission [14]. After these stages, intricate scattering processes involving the ejected solitons and DWs can take place [2]. These processes are also of key importance to explain the SC features [4–6].

Although SC generation was initially explained in these terms [1,2,14,15], Austin *et al.* pointed out that DWs are radiated before the soliton fission [19]. This is also in accordance with recent results in integrated waveguides [20, 21]. Interestingly, DW emission by pulses that propagate in the normal dispersion regime (called generalized DWs) has also been demonstrated [22, 23]. Despite the importance of new frequency generation processes triggered by soliton fission, these observations on DWs reveal that SC assisted by DW generation does not need pulse splitting, even when pumped in the anomalous dispersion regime. In these cases, the soliton dynamics is not essential and low-level strategies could be useful, in line with early interpretations of some SC spectra based on intrapulse FWM processes [24–26]. Here our aim is to obtain a unified analytical description of such DW emission, in both normal and anomalous dispersion regimes, through a low-level approach. Since numerical solutions of the NLSE are not required, our formalism provides, in addition, straightforward guidelines for designing SC sources.

An illustrative example of low-level descriptions has been the interpretation of DW emission by nearly nondispersive pulses in terms of cascaded FWM processes by Erkintalo *et al.* [27]. It did not only provide a deeper understanding of the radiation emitted by solitons, but also demonstrated that spectral resonances can be predicted without a complete solution for the NLSE. This work also reported the appearance of spectral resonances from pulses pumped in the normal dispersion regime close to the ZDF. Another very recent example has been the low-level analysis of the effective reflection of a weak linear wave induced by a soliton based on certain FWM processes [28, 29].

If frequency dispersion in time, *i.e.*, the dispersion of the instantaneous pulse frequency along the pulse duration, is significant, then new mechanisms can also arise [22]. In the normal dispersion regime, the optical wave-breaking (OWB) process can take place [30] provided the system is sufficiently nonlinear [31]. Conforti *et al.* studied this regime based on the shock-wave solution [3]. Although several cases can be understood from this high-level concept and some particular cases can be solved analytically [32], the group-velocity of the shock-wave must be numerically determined in general [3], which limits its applicability in design tasks. Recently, we proposed a combined approach where self-phase modulation (SPM) leading to OWB and DW emission mechanisms are studied based on the envelope evolution — a high-level concept — and discrete wave mixing — a low-level concept —, respectively [23]. *One* FWM process enabled by frequency dispersion in time and favored by a suitable HOD was identified for the DW emission, leading to an analytical expression that relates the position of the spectral resonance with the dispersion and the nonlinear coefficient of the waveguide and input pulse features. In this paper we extend our approach to new scenarios in both normal and anomalous dispersion regimes, where DWs are produced according to several FWM processes induced by the dispersion of frequencies in time.

The approach that we present in this paper will be applicable to both normal and anomalous dispersion regimes. This is in contrast with high-level formalisms which are fundamentally different for the normal and anomalous dispersion regimes because they rely on nonlinear envelope states. Particularly, these nonlinear states correspond to solitons in the anomalous dispersion case [1, 2, 14] and a shock-wave in the normal dispersion case [3, 32]. However, there are scenarios where a simple picture of the pulse as a coherent superposition of monochromatic

waves, that can disperse in time, can be suitable. In such cases, a unified approach for both the normal and anomalous dispersion regimes should be feasible [23, 27] and we here present such an approach for SC produced in scenarios that do not involve pulse splitting (thus before soliton fission occurs in the anomalous dispersion case [33, 34]).

In Section 2, we present a fully analytical approach to define key stages in the SC generation in both normal and anomalous dispersion regimes. We construct a picture of the frequency distribution in time based on these stages. In Section 3, several FWM processes are identified to produce direct and cascaded DW emission. This allows the derivation of analytical expressions that characterize the different scenarios and provide the resonance frequencies. Finally, Section 4 will be devoted to the application of this framework in actual (nonideal) waveguides. On the one side, an octave-spanning SC generation in a 2 mm-long foundry-compatible (220-nm-thick) silicon-on-insulator (SOI) strip waveguide [35] pumped at telecom wavelengths in the normal dispersion regime will be presented. On the other side, a recently reported SC spectrum obtained in a silicon nitride waveguide pumped in the anomalous dispersion regime [21] will be analyzed according to our framework.

2. A propagation equation for generalized lengths

A suitable definition of the different stages of the pulse evolution is extremely useful to depict a simplified, although consistent, model of the SC dynamics. The most extended scenario valid in the anomalous dispersion regime is composed of an initial pulse compression stage driven by SPM and anomalous group-velocity dispersion (GVD), followed by the soliton fission process due to higher-order effects (HOD, SRS or even noise) and subsequent radiation by the emerging solitons, and scattering processes involving such radiation and solitons [1,2]. Usually these stages are defined in terms of the changes experienced by the pulse (in both the time and frequency domains), thus requiring the numerical solution of the propagation equation. Nevertheless, such complete solutions contain information about the pulse details that is not essential to define the stages. This approach is not particularly efficient for determining the different SC stages, because the goal of defining these stages is precisely to provide a simpler analysis of the pulse evolution.

Such a simpler analysis can be enabled by looking for some properties of the pulse and its spectrum that allow the characterization of the propagation stages without solving numerically the NLSE. An intuitive example is given by the classical dispersive length, $L_{\mathrm{D}} = T_0^2/|\beta_2|$, where T_0 represents the pulse duration and β_2 is the GVD; and the nonlinear length, $L_{\mathrm{NL}} = 1/(\gamma_0 P_0)$, where γ_0 is the nonlinear coefficient and P_0 corresponds to the input pulse peak power. These parameters allow comparing the strength of the processes at work, namely, GVD and SPM (provided the pulse shape is not notably altered). Similarly, we recently proposed the generalized dispersive and nonlinear length functions, $\mathcal{L}_{\mathrm{D}}(z)$ and $\mathcal{L}_{\mathrm{NL}}(z)$, respectively, to extend this kind of analysis over the entire propagation distance [36]. For the convenience of the reader, we briefly review their meaning here. For the sake of clarity, let us consider the standard NLSE (although our remarks remain valid when HOD is included),

$$\partial_z \tilde{A}(z, \omega-\omega_0) = i\frac{\beta_2}{2}(\omega-\omega_0)^2 \tilde{A}(z,\omega-\omega_0) + i\gamma_0 \mathcal{F}_{\omega_0}^{-1}\left[|A(z,t)|^2 A(z,t)\right], \tag{1}$$

where ω_0 is the carrier frequency, $\tilde{f}(\omega-\omega_0) = \mathcal{F}_{\omega_0}[f(t)] = \int_{-\infty}^{\infty} \mathrm{d}t\, e^{i(\omega-\omega_0)t} f(t)$ is the Fourier transform centered at ω_0, and $\tilde{A}$ is the envelope of the analytic signal of the electric field [11]. Next we take averages of the right-hand side terms in Eq. (1) and introduce the following inverse length functions,

$$\mathcal{L}_{\mathrm{D}}^{-1}(z) = \frac{\beta_2}{2}\frac{\int_{-\infty}^{\infty} \mathrm{d}\omega\, (\omega-\omega_0)^2 |\tilde{A}(z,\omega-\omega_0)|^2}{\int_{-\infty}^{\infty} \mathrm{d}\omega\, |\tilde{A}(z,\omega-\omega_0)|^2}, \tag{2}$$

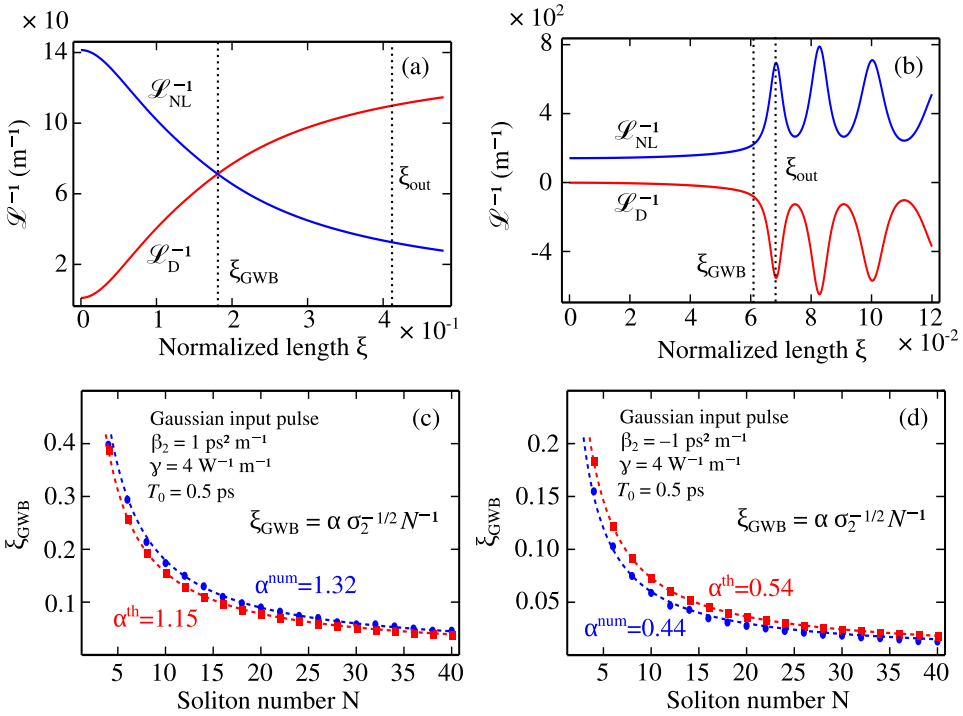

Fig. 1. (a)-(b): Evolution of the generalized lengths for $N = 10$ in (a) the normal dispersion and (b) the anomalous dispersion regimes. (c)-(d): Comparison of the analytically calculated (normalized) generalized wave-breaking distance (red squares) with the numerical results (blue circles) in (c) the normal dispersion and (d) the anomalous dispersion regimes. The parameters considered in theses cases are included in the insets of (c) and (d). See details of the formula for ξ_{GWB} in Table 1.

$$\mathcal{L}_{\mathrm{NL}}^{-1}(z) = \frac{\gamma_0}{2}\frac{\int_{-\infty}^{\infty} \mathrm{d}t\, |A(z,t)|^4}{\int_{-\infty}^{\infty} \mathrm{d}t\, |A(z,t)|^2}. \tag{3}$$

On the one hand, $\mathcal{L}_{\mathrm{D}}$ and $\mathcal{L}_{\mathrm{NL}}$ represent the length scales over which GVD and SPM, respectively, act at *any* z distance. On the other hand, the Hamiltonian conservation law [37] requires that $\mathcal{L}_{\mathrm{NL}}^{-1}(z)+\mathcal{L}_{\mathrm{D}}^{-1}(z) = \mathcal{L}_{\mathrm{NL}}^{-1}(0)+\mathcal{L}_{\mathrm{D}}^{-1}(0)$ [36]. This property allows the nonlinear pulse propagation to be interpreted as a competition between the generalized inverse lengths. Therefore, these functions can provide useful insight to identify the dynamic stages in the SC generation. Since Eq. (1) has actually one degree of freedom [37,38], parametrized by $N^2 = L_{\mathrm{D}}/L_{\mathrm{NL}} = T_0^2\gamma_0 P_0/\beta_2$, we from now on work with a normalized propagation distance, $\xi = z/L_{\mathrm{D}}$.

Figure 1(a) represents the typical evolution of $\mathcal{L}_{\mathrm{NL}}^{-1}$ and $\mathcal{L}_{\mathrm{D}}^{-1}$ in the normal dispersion regime [*i.e.*, $\mathrm{sign}(\beta_2) = 1$] when $\mathcal{L}_{\mathrm{NL}}^{-1}(0) \gg \mathcal{L}_{\mathrm{D}}^{-1}(0)$. The crosspoint at ξ_{GWB} (the — normalized — *generalized wave-breaking distance*) is a notable feature of this regime because it can define two stages without a full knowledge of the pulse envelope: Since $\mathcal{L}_{\mathrm{NL}}^{-1}(\xi) > \mathcal{L}_{\mathrm{D}}^{-1}(\xi)$ for $\xi < \xi_{\mathrm{GWB}}$, the spectral broadening (pointed out by the growth of $\mathcal{L}_{\mathrm{D}}^{-1}$, which is proportional to the variance of the spectral distribution) should be mainly driven by SPM in this stage. Moreover, $\mathcal{L}_{\mathrm{NL}}^{-1}$ captures the pulse broadening induced by $\beta_2 > 0$ through its decrease. For $\xi > \xi_{\mathrm{GWB}}$, dispersive effects should dominate the pulse propagation. Figure 1(b) corresponds to the anomalous dispersion regime [*i.e.*, $\mathrm{sign}(\beta_2) = -1$] also when $\mathcal{L}_{\mathrm{NL}}^{-1}(0) \gg \mathcal{L}_{\mathrm{D}}^{-1}(0)$. Although no crosspoint appears

in this case, again two different stages can also be identified in a natural way. The generalized lengths initially experience a relatively slowly varying monotonic evolution along ξ and evolve into an oscillatory behavior afterwards. Analogously to the previous case, the spectral broadening should be mainly induced by SPM initially. We point out that the pulse compression due to $\beta_2 < 0$ explains the growth of $\mathcal{L}_{\rm NL}^{-1}$. From this approach, no fundamental difference between the normal and anomalous dispersion regimes is observed. Similarly, the self-compression and self-decompression distances were also proposed without any particular distinction between the anomalous and normal regimes [34]. Therefore, we define the (normalized) generalized wave-breaking distance, $\xi_{\rm GWB}$, for both $\mathrm{sign}(\beta_2) = \pm 1$, as $\mathcal{L}_{\rm D}^{-1}(\xi_{\rm GWB}) = \mathrm{sign}(\beta_2)\mathcal{L}_{\rm NL}^{-1}(0)/2$. We will return later to the motivation of this definition (see next page). We now present a propagation equation for $\mathcal{L}_{\rm NL}^{-1}$ and, correspondingly, for $\mathcal{L}_{\rm D}^{-1}$.

We take only two effects into account to determine the evolution of the generalized lengths for $\xi < \xi_{\rm GWB}$. Firstly, we assume that SPM rules the spectral broadening in this stage. This assumption is expected to be completely valid when $\mathcal{L}_{\rm NL}^{-1}(0) \gg \mathcal{L}_{\rm D}^{-1}(0)$. Secondly, we neglect any pulse reshaping and consider an effective broadening or compression in time (see Appendix). Based on Eq. (1) and keeping in mind these assumptions, we derive in Appendix

$$\frac{\mathrm{d}}{\mathrm{d}\xi}\left[\frac{\mathcal{L}_{\rm NL}^{-1}(\xi)}{\mathcal{L}_{\rm NL}^{-1}(0)}\right] = -2\, s_2\, N \left[\frac{\mathcal{L}_{\rm NL}^{-1}(\xi)}{\mathcal{L}_{\rm NL}^{-1}(0)}\right]^2 \left(s_2\,\sigma_2\left[1 - \frac{\mathcal{L}_{\rm NL}^{-1}(\xi)}{\mathcal{L}_{\rm NL}^{-1}(0)}\right]\right)^{1/2}, \tag{4}$$

where σ_2 is an input-pulse form factor (see its value in the caption of Table 1 and details in Appendix), and $s_2 = \mathrm{sign}(\beta_2)$. To check the validity of Eq. (4), first we numerically solve Eq. (1) to obtain $\xi_{\rm GWB}$ according to its definition. Then we analytically solve Eq. (4) and impose $\mathcal{L}_{\rm NL}^{-1}(\xi_{\rm GWB}) = (1 - s_2/2)\mathcal{L}_{\rm NL}^{-1}(0)$, so that we obtain

$$\xi_{\rm GWB} = \frac{s_2}{2\,N\,\sigma_2^{1/2}} \int_{1-s_2/2}^{1} \frac{\mathrm{d}a}{a^2\,[s_2(1-a)]^{1/2}}. \tag{5}$$

In Fig. 1(c) and Fig. 1(d) we compare the analytical results based on Eq. (5) with those evaluated numerically. Despite the assumptions made in Eq. (4), good agreement is observed. This indicates that our approximations (see Appendix) are in accordance with the conditions of the scenarios illustrated in Fig. 1.

For $\xi > \xi_{\rm GWB}$, the dynamics become notably different in Figs.1(a) and 1(b). In both regimes, $\mathcal{L}_{\rm D}^{-1}$ strengthens as the pulse propagates. It also indicates that, besides the spectral broadening, frequency dispersion starts to play a more important role. It is well-known that in the normal dispersion regime, the dispersion can produce frequency overtaking in the pulse tails that leads to strong oscillations in the pulse intensity. This phenomenon was interpreted early on as shock-wave formation and OWB [30, 31, 39, 40]. Furthermore, the observation of these oscillations has been greatly improved very recently by means of an optical sampling oscilloscope [41]. Interestingly, although shock-wave formation enables nonlinear mixing involving frequencies in the pulse tails [3,23,31,32], these mixing processes could also appear due to a partial overlapping. From this point of view, shock-wave and OWB would be extreme cases of frequency overlapping in time. The latter suggests that the GVD-induced spreading in time of frequencies generated initially by SPM can enable new nonlinear mixing between these frequencies in both normal and anomalous dispersion regimes, the only difference between the two cases being the frequencies involved: in the normal dispersion regime, it are those contained in the pulse tails, $(\omega_{\rm SPM}^{-}, \omega_0)$ or $(\omega_0, \omega_{\rm SPM}^{+})$; and, in the anomalous dispersion regime, it are those contained in the central part of the pulse, $(\omega_{\rm SPM}^{-}, \omega_{\rm SPM}^{+})$, where $\omega_{\rm SPM}^{\pm} = \omega_0 \pm \delta\omega_{\rm SPM}$ with $\delta\omega_{\rm SPM}$ representing the maximum SPM-induced chirp (see Fig. 2). This similar treatment for both dispersion regimes motivates the definition of one generalized wave-breaking distance. When using this definition, one has to

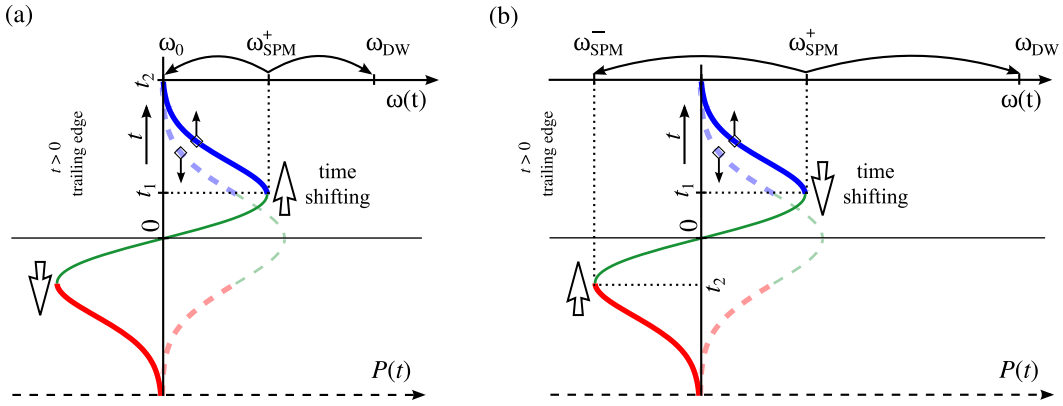

Fig. 2. Illustration of the frequency overlapping and the resulting FWM processes in (a) the normal dispersion regime, $s_2 = 1$, and (b) the anomalous dispersion regime, $s_2 = -1$. The schematic plots include the absolute instantaneous frequency, $\omega(t) = \omega_0 + \delta\omega(t)$ (continuous lines), and instantaneous power, $P(t)$ (dashed lines). Thick lines highlight the frequencies that can overlap. The time shifting induced by dispersion can induce the FWM processes that are represented.

take into account that in the normal case the spectral broadening due to SPM is mainly produced before ξ_{GWB}, whereas in the anomalous case, due to the pulse compression, $\mathcal{L}_{\mathrm{NL}}^{-1}$, and therefore SPM, experiences the most important growth just after ξ_{GWB}. Clearly, this feature cannot be neglected in a reasonable model.

From Eq. (4), we can estimate the frequencies that could interact in the second stage (*i.e.*, $\xi > \xi_{\mathrm{GWB}}$), provided the distance at which frequency overlapping takes place, ξ_{ol}, is known. In the anomalous dispersion scenario [see Fig. 1(b)] the distance at which $\mathcal{L}_{\mathrm{NL}}^{-1}$ attains its first maximum, $\mathcal{L}_{\mathrm{NL}}^{-1}(\xi_{\mathrm{ol}}) = \max(\mathcal{L}_{\mathrm{NL}}^{-1})$, could be an appropriate choice because it is related to the maximum compression distance in the time domain and hence maximum frequency overlapping. In contrast, it is not straightforward to define such a distance in the normal dispersion case. Based on the above qualitative description of ξ_{ol}, the pulse broadening at ξ_{ol} can be estimated to be roughly twice that attained at ξ_{GWB}. Consequently, in the normal dispersion scenario, we define $\mathcal{L}_{\mathrm{NL}}^{-1}(\xi_{\mathrm{ol}}) = \mathcal{L}_{\mathrm{NL}}^{-1}(\xi_{\mathrm{GWB}})/2$. Note that the aim of defining ξ_{ol} is to facilitate evaluating the frequency ranges that will be involved in the nonlinear mixing in the second stage.

Let us first analyze the anomalous dispersion case. Equation (4) takes into account SPM and pulse compression induced by GVD. As a result, it predicts that $\mathcal{L}_{\mathrm{NL}}^{-1}$ diverges for $\xi > \xi_{\mathrm{GWB}}$. Obviously, it is an artificial divergence as we can observe in Fig. 1(b). In fact, for $\xi > \xi_{\mathrm{ol}}$, the pulse experiences both spectral and temporal narrowing and broadening, hence avoiding any divergence or pulse collapse. The physical reasons explaining that behavior are analogous to those accounting for the maximum pulse compression of a positively chirped pulse in a linear waveguide with anomalous dispersion [38]. Indeed, a clear similarity with the case we are dealing with arises, the SPM-induced chirp playing the role of the initial positive chirp in the linear case. Furthermore, this analogy suggests the following strategy to evaluate the spectral broadening at ξ_{ol}: if we define a chirped Gaussian pulse at ξ_{GWB} satisfying $\mathcal{L}_{\mathrm{D}}^{-1}(\xi_{\mathrm{GWB}}) = \mathrm{sign}(\beta_2)\mathcal{L}_{\mathrm{NL}}^{-1}(0)/2$, then we can estimate $\mathcal{L}_{\mathrm{NL}}^{-1}(\xi_{\mathrm{ol}})$ as defined above from the analytical results of the linear case (see Appendix). Once $\mathcal{L}_{\mathrm{NL}}^{-1}(\xi_{\mathrm{ol}})$ is known, both ξ_{ol} and the range of frequencies eventually overlapping can be estimated through an extrapolation of Eq. (4).

A similar approximation can be applied in the normal dispersion regime, but then considering that $\mathcal{L}_{\mathrm{NL}}^{-1}(\xi_{\mathrm{ol}}) = \mathcal{L}_{\mathrm{NL}}^{-1}(0)/4$. A synopsis of the most important analytical results presented here

Table 1. Characteristic lengths, ξ_{GWB} and ξ_{ol}, and the maximum chirps generated by SPM at such lengths. Here a can be considered an auxiliary variable, σ_2, and Υ are input-pulse form factors. In particular, they equal to 16/35 and $4/\sqrt{27}$, respectively, for a sech pulse and $\sqrt{8/27}$ and $\sqrt{2/e}$ for a Gaussian pulse. $\tilde{\sigma}_2$ is an auxiliary parameter equals to $1/\sqrt{2}$ (see details in Appendix). Remember that $N^2 = L_{\mathrm{D}}/L_{\mathrm{NL}}$.

	Normal dispersion regime, $\beta_2 > 0$	Anomalous dispersion regime, $\beta_2 < 0$
a_{GWB}	$\dfrac{1}{2}$	$\dfrac{3}{2}$
ξ_{GWB}	$\dfrac{1}{2N\,\sigma_2^{1/2}}\displaystyle\int_{a_{\mathrm{GWB}}}^{1}\dfrac{\mathrm{d}a}{a^2(1-a)^{1/2}} \approx \dfrac{1.15}{N\,\sigma_2^{1/2}}$	$\dfrac{1}{2N\,\sigma_2^{1/2}}\displaystyle\int_{1}^{a_{\mathrm{GWB}}}\dfrac{\mathrm{d}a}{a^2(a-1)^{1/2}} \approx \dfrac{0.54}{N\,\sigma_2^{1/2}}$
$\delta\omega_{\mathrm{GWB}}$	$\dfrac{1}{\sqrt{2}}\dfrac{\Upsilon}{\sigma_2^{1/2}}\dfrac{N}{T_0}$	$\dfrac{1}{\sqrt{2}}\dfrac{\Upsilon}{\sigma_2^{1/2}}\dfrac{N}{T_0}$
a_{ol}	$\dfrac{1}{4}$	$\dfrac{3}{2}\left(1+\dfrac{2}{9}\dfrac{N^2}{\tilde{\sigma}_2}\right)^{1/2}$
ξ_{ol}	$\dfrac{1}{2N\,\sigma_2^{1/2}}\displaystyle\int_{a_{\mathrm{ol}}}^{1}\dfrac{\mathrm{d}a}{a^2(1-a)^{1/2}}$	$\dfrac{1}{2N\,\sigma_2^{1/2}}\displaystyle\int_{1}^{a_{\mathrm{ol}}}\dfrac{\mathrm{d}a}{a^2(a-1)^{1/2}}$
$\delta\omega_{\mathrm{ol}}$	$\delta\omega_{\mathrm{GWB}} + \dfrac{1}{4\sqrt{2}T_0}\left(1+\dfrac{2N^2}{\tilde{\sigma}_2}\right)(\xi_{\mathrm{ol}}-\xi_{\mathrm{GWB}})$	$\dfrac{\Upsilon}{\sigma_2^{1/2}}\dfrac{N}{T_0}\,(a_{\mathrm{ol}}-1)^{1/2}$

and derived in Appendix is shown in Table 1. We use these results in the next section, where several scenarios that exploit DW emission to generate SC are identified.

3. Direct and cascaded dispersive wave emission

The analysis of the generalized lengths allows identifying the frequencies that can overlap, thus can generate new frequencies through FWM in the second stage, after ξ_{GWB} (see Table 1). We now study new frequency production through direct processes, *i.e.*, one FWM interaction fed by SPM (both pump and signal waves generated in the first stage by SPM), but also through cascaded processes, *i.e.*, FWM interactions fed by other FWM processes also produced in the second stage. As will be shown soon, direct DW emission can take place in waveguides with, in addition to GVD, third-order dispersion, while cascaded processes require third and fourth-order dispersion. Equation (1) must then be extended, in which case it is called generalized NLSE (GNLSE),

$$\partial_z \tilde{A}(z,\omega-\omega_0) = i\beta_p(\omega)\tilde{A}(z,\omega-\omega_0) + i\gamma_0\mathcal{F}_{\omega_0}^{-1}\left[|A(z,t)|^2\,A(z,t)\right], \tag{6}$$

where $\beta_p(\omega) = \beta(\omega)-\beta_1(\omega-\omega_0)-\beta_0 = \sum_{k=2}\beta_k(\omega-\omega_0)^k/k!$, with $\beta_k = \mathrm{d}^k\beta/\mathrm{d}\omega^k|_{\omega_0}$ [1,38].

The evolution of the generalized lengths is assumed to be ruled by SPM and GVD and the most important effect of HOD is to favor specific FWM processes in the second stage. In this section we pursue to determine the HOD, and therefore the waveguide dispersion curve, that induces DW emission at targeted frequencies to further enhance the pulse spectral broadening in the second propagation stage. Consequently, at this point, the FWM processes to be exploited must be selected *a priori* to derive the HOD.

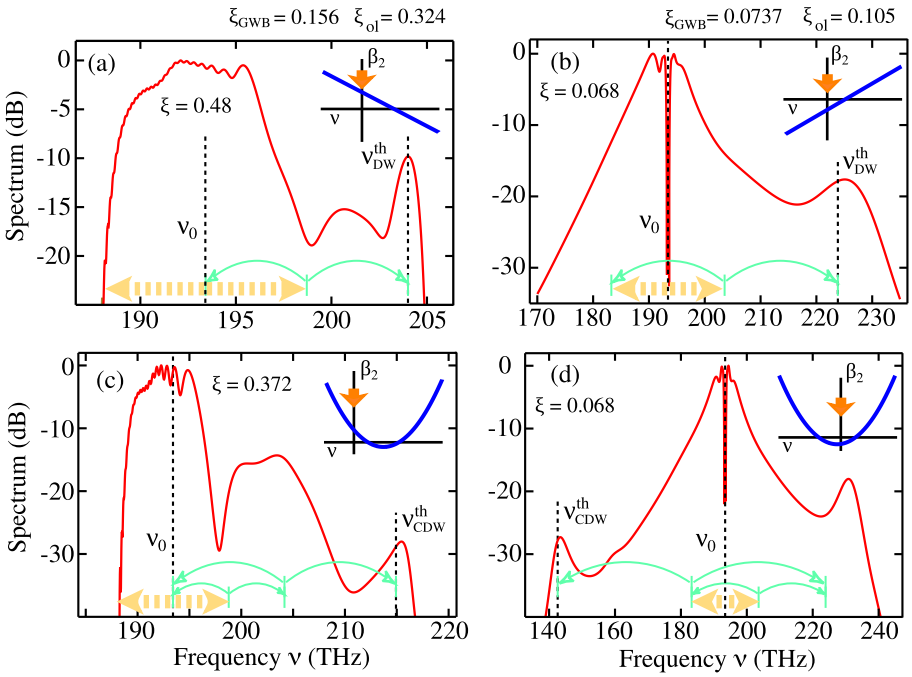

Fig. 3. Direct DW emission in (a) the normal regime and (b) the anomalous regime. Cascaded DW emission in (c) the normal regime and (d) the anomalous regime. HOD has been calculated according to the analytical results in Table 2 using $\delta\omega_{\mathrm{SPM}} = \delta\omega_{\mathrm{ol}}$ and $|\beta_2| = 1\,\mathrm{ps^2 m^{-1}}$, $\gamma_0 = 4\,\mathrm{W^{-1} m^{-1}}$, $T_0 = 0.5\,\mathrm{ps}$ and ν_0 corresponding to 1550 nm. The position of the resonances are successfully predicted in our framework in all these cases. The propagations have been stopped at the distances ξ, where the resonances achieve their maximum power levels while additional processes not included in our model have not impacted the dynamics yet. Yellow dashed arrows represent the spectral broadening relying on SPM and green solid arrows indicate the FWM processes that have been considered. The dispersion profiles, including arrows to indicate the pumping frequency, have been added as insets.

First, we address direct DW emission in the normal dispersion regime. Among the two ranges of frequencies that get closer in the time domain due to the GVD [*e.g.*, the frequency range present in the trailing pulse edge $(\omega_0, \omega^+_{\mathrm{SPM}})$], the FWM process $2\,\omega^+_{\mathrm{SPM}} \rightarrow \omega_0 + \omega_{\mathrm{DW}}$ with ω^+_{SPM} as pump and ω_0 as signal [see Fig.2(a)] is more favorable in terms of power [see Fig. 2(a), $P(t_1) \gg P(t_2)$] than the reciprocal process where ω_0 acts as pump wave and ω^+_{SPM} as signal wave. Consequently, new frequency generation is expected to be more pronounced through the former channel. [The same considerations can be applied to the range $(\omega^-_{\mathrm{SPM}}, \omega_0)$ and the process $2\,\omega^-_{\mathrm{SPM}} \rightarrow \omega_0 + \omega_{\mathrm{DW}}$.] In addition, it can provide the highest (lowest) new frequency. If phase matching is imposed in this process, then $\beta(\omega_{\mathrm{DW}}) + \beta(\omega_0) - 2\beta(\omega^+_{\mathrm{SPM}}) = \beta_2(\omega^+_{\mathrm{SPM}})[\delta\omega_{\mathrm{SPM}}]^2 = 0$ (the nonlinear phase mismatch is assumed to be negligible) when dispersion up to the third-order (β_3) is considered [38]. As a result, the phase matching condition can be rewritten as $\beta_3 = -\beta_2/\delta\omega_{\mathrm{SPM}}$, as we already reported in [23]. Note that the FWM pump frequency, ω^+_{SPM} (or ω^-_{SPM}), corresponds, in this case, to the ZDF, in line with previous experimental works where spectral peaks were observed when using input pump pulses at normal dispersion regime [26, 42]. Interestingly, this condition also leads to a group-velocity matching between the signal and idler waves involved in this FWM process, $\beta_1(\omega_0) = \beta_1(\omega_{\mathrm{DW}})$. Therefore, in this case, both phase matching and group-velocity matching can be attained simultaneously by means of just one additional degree of

freedom, namely, that related to β_3. If group-velocity dispersion allows space-time overlapping as described above and phase matching permits gain in the nonlinear FWM process, group-velocity matching becomes important to sustain the intrapulse frequency conversion [24, 42]. In Fig. 3(a), we show the numerical solutions of Eq. (6) for the system described in Fig. 1(a) with β_3 given by the corresponding expression collected in Table 2 and $\delta\omega_{\mathrm{SPM}} = \delta\omega_{\mathrm{ol}}$ (see Table 1). An excellent agreement is observed between the idler wave frequency produced through the above mentioned FWM process, $\nu_{\mathrm{DW}}^{\mathrm{th}}$, and the frequency of the spectral resonance appearing in the numerical simulation.

Second, we study direct DW emission in the anomalous dispersion regime, where GVD induces frequency overlapping between the frequencies $(\omega_{\mathrm{SPM}}^{-}, \omega_{\mathrm{SPM}}^{+})$ because $\beta_2 < 0$. In this case, we focus on $2\,\omega_{\mathrm{SPM}}^{+} \rightarrow \omega_{\mathrm{SPM}}^{-} + \omega_{\mathrm{DW}}$ [or $2\,\omega_{\mathrm{SPM}}^{-} \rightarrow \omega_{\mathrm{SPM}}^{+} + \omega_{\mathrm{DW}}$]. The phase matching requirement corresponds to $\beta(\omega_{\mathrm{DW}}) + \beta(\omega_{\mathrm{SPM}}^{-}) - 2\beta(\omega_{\mathrm{SPM}}^{+}) = \beta_2(\omega_{\mathrm{SPM}}^{+})[2\delta\omega_{\mathrm{SPM}}]^2 = 0$, and again it leads to $\beta_3 = -\beta_2/\delta\omega_{\mathrm{SPM}}$ and to group-velocity matching between waves that take part in this process, $\beta_1(\omega_{\mathrm{SPM}}^{-}) = \beta_1(\omega_{\mathrm{DW}})$. Analogously to the direct DW emission in the normal dispersion regime, the FWM pump frequency corresponds to the ZDF, similarly to [24].

When comparing the idler frequency analytically determined, indicated by $\nu_{\mathrm{DW}}^{\mathrm{th}}$, with the spectral resonance obtained numerically in Fig. 3(b), we again observe a good agreement.

Next we study some cascaded scenarios keeping in mind the idea of maximizing the spectral broadening. It is known that a cascade can be induced through nonresonant intermediate processes [27]. In the normal dispersion regime, we aim to get $2\,\omega_{\mathrm{SPM}}^{+} \rightarrow \omega_0 + \omega_{\mathrm{i}}$ (ω_{i} is not necessarily resonant), and subsequently $2\,\omega_{\mathrm{i}} \rightarrow \omega_0 + \omega_{\mathrm{CDW}}$. Therefore, if only phase matching and group-velocity matching on the last process of our cascade, $2\,\omega_{\mathrm{i}} \rightarrow \omega_0 + \omega_{\mathrm{CDW}}$, is considered, $\beta(\omega_{\mathrm{CDW}}) + \beta(\omega_0) - 2\beta(\omega_{\mathrm{i}}) = \beta_2(\omega_{\mathrm{i}})[2\delta\omega_{\mathrm{SPM}}]^2 + (1/12)\beta_4[2\delta\omega_{\mathrm{SPM}}]^4 = 0$ [38] and $\beta_1(\omega_0) = \beta_1(\omega_{\mathrm{i}})$. Note that, in this case, the group-velocity matching involves the pump and signal waves of the second process of the cascade. These conditions lead to $\beta_3 = -5\beta_2/3\delta\omega_{\mathrm{SPM}}$ and $\beta_4 = \beta_2/\delta\omega_{\mathrm{SPM}}^2$. We want to exploit this process with as few requirements as possible. As such, a GNLSE with one additional degree of freedom, that linked to β_4, is used. The numerical output spectrum plotted in Fig. 3(c) shows a resonance in line with the theoretical position of the cascaded DW, $\nu_{\mathrm{CDW}}^{\mathrm{th}}$.

The cascade studied in the anomalous dispersion regime includes the following processes: $2\,\omega_{\mathrm{SPM}}^{+} \rightarrow \omega_{\mathrm{SPM}}^{-} + \omega_{\mathrm{i}}$ and $2\,\omega_{\mathrm{SPM}}^{-} \rightarrow \omega_{\mathrm{i}} + \omega_{\mathrm{CDW}}$. Similarly to the previous case, we impose $\beta(\omega_{\mathrm{CDW}}) + \beta(\omega_{\mathrm{i}}) - 2\beta(\omega_{\mathrm{SPM}}^{-}) = \beta_2(\omega_{\mathrm{SPM}}^{-})[4\delta\omega_{\mathrm{SPM}}]^2 + (1/12)\beta_4[4\delta\omega_{\mathrm{SPM}}]^4 = 0$ and $\beta_1(\omega_{\mathrm{SPM}}^{-}) = \beta_1(\omega_{\mathrm{i}})$. In this case, we derive $\beta_3 = -2\beta_2/9\delta\omega_{\mathrm{SPM}}$ and $\beta_4 = -2\beta_2/3\delta\omega_{\mathrm{SPM}}^2$. The numerically simulated resonance observed in Fig. 3(d) again corresponds well with the theoretical $\nu_{\mathrm{CDW}}^{\mathrm{th}}$. This agreement in several and notably different scenarios strongly supports our approach as a valid tool to address SC generation relying on SPM and DW emission.

Note that the HOD used here served to stimulate a resonance at ω_{CDW} and a spectral peak has appeared there according to our theory. Nevertheless, other resonant processes can also occur; in fact, an additional resonance is excited in this scenario, contributing to the spectral broadening. From this point of view, the above results indicate that the expressions in Table 2 (including the information provided by Table 1) represent *sufficient* conditions to *efficiently* induce DWs. Note that, regarding design tasks, this is the most useful information. Furthermore, the analysis of phase and group-velocity matching, *i.e.*, the conditions leading to the results in Table 2, can also improve the understanding of any DW emission. To illustrate this, the following section will be devoted to the analysis of all the spectral resonances appearing in the numerically calculated spectra in actual waveguides. That strategy is also valid to interpret the high- frequency resonance in Fig. 3(d).

It is worth remarking that, in the anomalous dispersion regime, DW formation is often interpreted based on the coupling between a soliton and linear waves [2, 14, 15, 19]. This high-level theory assumes an *ansatz* to Eq. (6) that consists of two parts: a solution to Eq. (1) that belongs to the family of fundamental solitons and a small-amplitude linear wave [2, 4, 13, 38].

After neglecting the nonlinear coupling terms in the resulting equation as indicated in [4, 13], the following phase matching condition is derived, $\beta(\omega_{\mathrm{DW}}) = \beta_0 + \beta_1(\omega_{\mathrm{DW}} - \omega_0)$ (in case one neglects the nonlinear contribution to the soliton wavenumber). Interestingly, our framework can explain this *ansatz* because the distance at which $\mathcal{L}_{\mathrm{NL}}^{-1}$ attains its first maximum is related to the distance where the pulse chirp becomes zero. As a result, a generalized fundamental soliton can be identified around this distance (the self-compression point) due to its straight-line dispersion curve. Moreover, our approach also identifies FWM (low-level) processes capable of emitting DWs and conditions allowing efficient radiation. (Note that we do not impose group-velocity matching between the soliton and the DW, but it affects waves involved in the FWM process that is selected.)

We would like to stress that the new physical insights obtained from our approach also pave the way to an *inverse nonlinear engineering*. The procedure hereto can be outlined in three steps. In the first one, the *inverse nonlinear design* step, the results above can be used to obtain the optimal dispersive features of a waveguide exhibiting a given nonlinear response: From the available input pulse (pulse shape, N and center wavelength), Table 1 and Table 2 determine the dispersion curves and the characteristic distances associated to several possible scenarios. The desired output spectral bandwidth, the features of the available pump source, and the degrees of freedom for the waveguide design will determine the most convenient scenario to be selected. In the second step, the *inverse linear design* step, a waveguide cross-section is obtained from the target dispersion curve defined in the previous step [45]. Finally, once a suitable waveguide is found, and $\beta(\omega)$ and $\gamma(\omega)$ have been calculated, the GNLSE, including higher-order effects, is numerically solved in order to check the output spectrum of the realistic waveguide design [23].

Most of the times, the target dispersion could not be exactly realized with realistic waveguide cross-sections. For example, the waveguide thickness is often constrained in photonic fabrication foundries. Then dispersion control is restricted to the optimization of a few number of parameters (*e.g.*, the waveguide width [43]) and consequently, dispersion engineering is limited. Even in these cases, Table 1 and Table 2 provide valuable information since it sets a target that should be realized as closely as possible with the dispersion engineering possibilities at hand. What is more, our framework can also be helpful to understand the origin of spectral resonances produced in a waveguide that does not feature exactly the HOD presented in Table 2. To illustrate the latter, we apply our framework to concrete SC examples based on waveguides that have been already fabricated.

4. Supercontinuum relying on generalized wave-breaking: case studies

Designing a new octave-spanning SC source in a 220 nm-thick silicon waveguide pumped at 1550 nm

As a first case study, we use our framework for designing a SC source based on a SOI strip waveguide with a fixed thickness of 220 nm, in line with the fabrication rules of multi-project wafer runs of photonic foundries [46]. From the dispersion profile in [47] for such a foundry-compatible (*i.e.*, 220 nm-thick) SOI waveguide with a width of 900 nm, we can derive that the type of scenario corresponding to Fig. 3(c) could be feasible in that waveguide [see inset in Fig. 4(a)]. Guided by Table 1, we consider 50 fs-long sech pump pulses with 150 W of peak power at 1550 nm. Figure 4(a) shows the octave-spanning output spectrum after propagation through this waveguide along 2 mm. The solid blue curve is the simulated spectrum taking into account linear losses of 2 dB cm^{-1} [43], two-photon absorption (TPA), the dispersion of the nonlinear coefficient [23, 48, 49], free-carrier-related effects and SRS [43] and the spectrum without these higher-order effects but with an effective nonlinear coefficient [23] is indicated by the green dashed curve. Common features between Fig. 4(a) and Fig. 3(c) become apparent. Consequently, we analyze the output spectrum in Fig. 4(a) keeping in mind the dynamics corresponding to Fig. 3(c).

Table 2. Four different scenarios for SC relying on direct and cascaded DW. The optimal HOD parameters that induces group-velocity matching and phase matching for those FWM and the spectral broadening produced through each mechanism (ω_{DW} or ω_{CDW}) are also included. $\delta\omega_{\mathrm{SPM}}$ can be estimated by $\delta\omega_{\mathrm{ol}}$ in Table 1.

$\mathrm{sign}(\beta_2)$	Favored FWM processes	β_3	β_4	$\omega_{\mathrm{DW\|CDW}} - \omega_0$	Example
1	$2\,\omega^{+}_{\mathrm{SPM}} \rightarrow \omega_0 + \omega_{\mathrm{DW}}$	$-\dfrac{\beta_2}{\delta\omega_{\mathrm{SPM}}}$	0	$2\,\delta\omega_{\mathrm{SPM}}$	Fig. 3(a)
1	$\begin{cases} 2\,\omega^{+}_{\mathrm{SPM}} \rightarrow \omega_0 + \omega_{\mathrm{i}} \\ 2\,\omega_{\mathrm{i}} \rightarrow \omega_0 + \omega_{\mathrm{CDW}} \end{cases}$	$-\dfrac{5}{3}\dfrac{\beta_2}{\delta\omega_{\mathrm{SPM}}}$	$\dfrac{\beta_2}{\delta\omega^2_{\mathrm{SPM}}}$	$4\,\delta\omega_{\mathrm{SPM}}$	Fig. 3(c)
-1	$2\,\omega^{+}_{\mathrm{SPM}} \rightarrow \omega^{-}_{\mathrm{SPM}} + \omega_{\mathrm{DW}}$	$-\dfrac{\beta_2}{\delta\omega_{\mathrm{SPM}}}$	0	$3\,\delta\omega_{\mathrm{SPM}}$	Fig. 3(b)
-1	$\begin{cases} 2\,\omega^{+}_{\mathrm{SPM}} \rightarrow \omega^{-}_{\mathrm{SPM}} + \omega_{\mathrm{i}} \\ 2\,\omega^{-}_{\mathrm{SPM}} \rightarrow \omega_{\mathrm{i}} + \omega_{\mathrm{CDW}} \end{cases}$	$-\dfrac{2}{9}\dfrac{\beta_2}{\delta\omega_{\mathrm{SPM}}}$	$-\dfrac{2}{3}\dfrac{\beta_2}{\delta\omega^2_{\mathrm{SPM}}}$	$-5\,\delta\omega_{\mathrm{SPM}}$	Fig. 3(d)

The inverse generalized lengths, $\mathcal{L}_{\mathrm{NL}}^{-1}$ and $\mathcal{L}_{\mathrm{D}}^{-1}$, in Fig. 4(b) evolve similarly as in Fig. 1(a). They also provides valuable information about propagation distances of interest. In the first stage ($z < z_{\mathrm{GWB}}$), SPM broadens the spectrum. The analysis of the relative group velocity, $\beta_1(\omega) - \beta_1(\omega_0)$, in Fig. 4(c) allows identifying which frequencies generated through SPM in the first stage could overlap due to their GVD in the second stage ($z > z_{\mathrm{GWB}}$). In this case, red-shifted frequencies, $\omega < \omega_0$ with $\beta_1(\omega) < \beta_1(\omega_0)$ (indicated in the green background), tend to approach ω_0 in the leading pulse edge [see also Fig. 2(a)]. Among the FWM processes favored by the frequency-dispersion-induced overlapping, those allowed by energy conservation and phase matching [see Fig. 4(d)] can extend the spectral broadening initiated by SPM. Note that the spectrum spans an octave through this mechanism also in the realistic simulation that includes all effects in the silicon waveguide [see solid blue line in Fig. 4(a)].

Moreover, based on Section 3, spectral resonances arise if both phase matching and group-velocity matching are fulfilled. Phase matching can be evaluated through the linear phase mismatch, $\Delta\beta = \beta(\omega_i) + \beta(\omega_s) - 2\beta(\omega_p)$, of the degenerate FWM processes that can take place, $2\,\omega_p \rightarrow \omega_s + \omega_i$. Unlike the group-velocity matching, the phase-matching condition depends on linear and nonlinear contributions. Although the linear phase mismatch can be readily evaluated, the nonlinear term would require details of the pulse due to its dynamical nature. For these reasons, we choose to restrict our study to $\Delta\beta$, while keeping in mind an uncertainty related to the nonlinear mismatch. This analysis is done in Fig. 4(d). In addition, the solid green line that intersects with "S" in this figure relates the pump and signal waves involved in processes with group-velocity matching between pump and signal waves. Accordingly, the spectral resonance ω_{CDW} can be interpreted as the idler of a FWM process involving the pump and signal waves depicted as "P" and "S", respectively. This is in agreement with our analysis in Fig. 3(c).

It is worth reminding that group-velocity and phase matching are conditions allowing *efficient* FWM. Notwithstanding, new frequency generation can also take place if these requirements are not fulfilled provided pump and signal waves can interact. These processes, besides broadening the spectrum, can also feed other FWM interactions, the second step in cascaded processes [*e.g.*, $2\omega_i \rightarrow \omega_0 + \omega_{\mathrm{CDW}}$ in Fig. 3(c) and Table 2]. Indeed, these processes can contribute to the pump wave "P" production according to Fig. 4(d). Of course, higher-order effects, *e.g.*, nonlinear losses, can affect these processes. The comparison between the green dashed and blue solid lines in Fig. 4(a) indicates the position of ω_{CDW} is not altered, but its efficiency is reduced (as expected

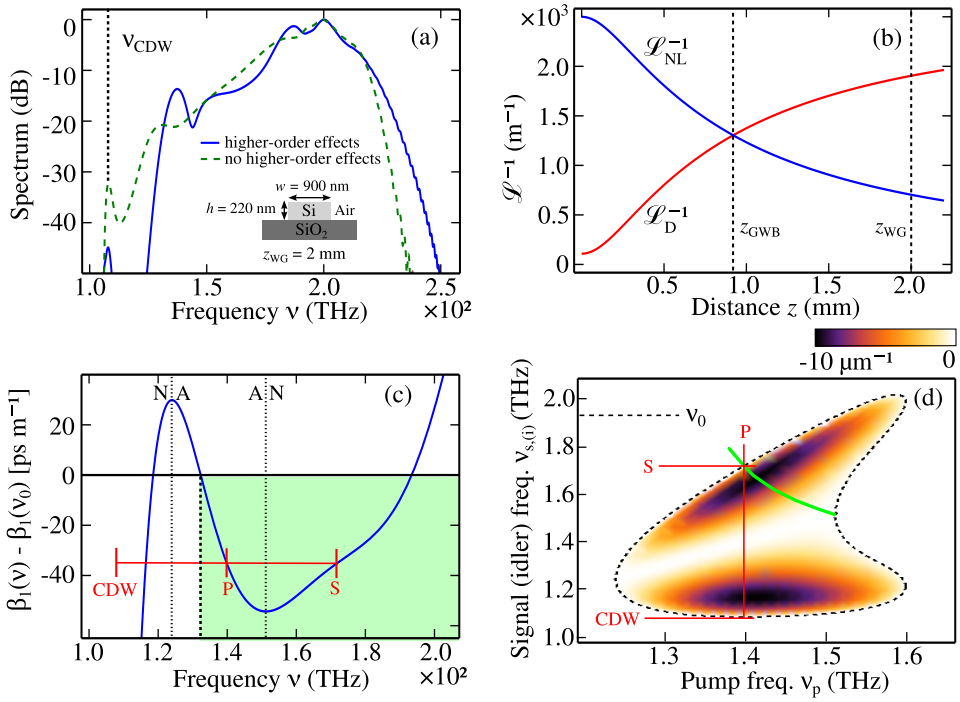

Fig. 4. (a) Output spectra simulated through Eq. (6) including higher order effects (blue solid curve) and without them (green dashed line). (b) Evolution of the generalized lengths [*cf.* Fig. 1(a)]. (c) Plot of the relative β_1, *i.e.*, the inverse of the group velocity. The green window includes the frequencies that can overlap in the leading pulse edge. A and N indicate anomalous and normal dispersion, respectively. (d) Linear phase mismatch (only negative values are represented). The green solid curve points out processes with group-velocity matching (see details in the text).

due to TPA) and new resonant processes become more efficient (see the spectral peak around 140 THz).

This example shows the (nearly unexplored) potential of pumping in the normal dispersion regime to produce broadband light in silicon waveguides compared to previous approaches pumping in the anomalous dispersion regime [20, 43, 50]. It can represent an important breakthrough towards the experimental demonstration of an octave-spanning SC spectrum in silicon pumping in the short-wavelength infrared since, according to our knowledge, it has only been achieved in SOI waveguides pumping beyond 2.2 μm, *i.e.*, above the TPA threshold of silicon [44].

Analyzing SC results in literature

As a second example of how to use our framework in practice, we analyze the dynamics of the experimental SC reported recently in [21]. There a silicon nitride waveguide was used, pumped in the anomalous dispersion regime with 92 fs-long Gaussian pulses with 260 W of peak power at 1030 nm. In Fig. 5(a), we show the spectra at different distances, including the output spectrum corresponding to Fig. 2 of [21]. We numerically calculate the evolution of the generalized lengths for this system and plot the result in Fig. 5(b). The behavior of the generalized lengths resembles that in Fig. 1(b) and the total waveguide length (z_{WG} = 8 mm) is slightly beyond the distance where $\mathscr{L}^{-1}_{NL}$ attains its first maximum. Whereas the generalized lengths in Fig. 5(b) and Fig. 1(b) are similar, the features of the spectrum in Fig. 5(a) strongly suggest that it is related to the

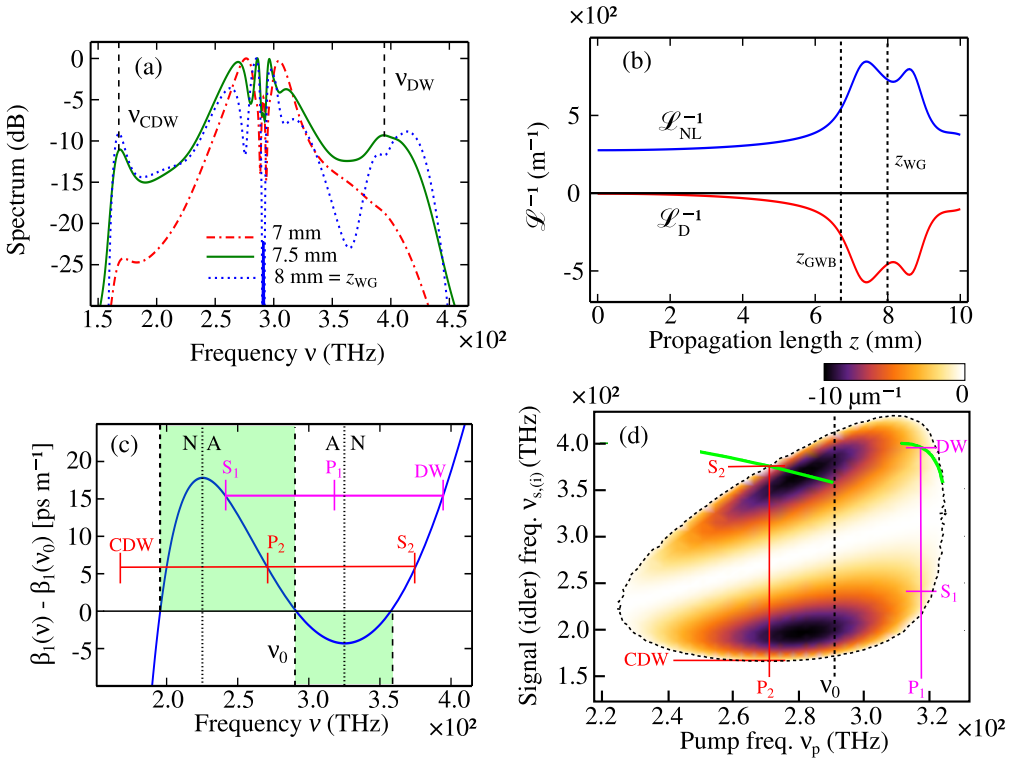

Fig. 5. (a) Output spectra at several distances between z_{GWB} and the total length of the waveguide, z_{WG}, according to [21]. (b) Evolution of the generalized lengths [*cf.* Fig. 1(b)]. (c) Plot of the relative β_1, *i.e.*, the inverse of the group velocity. The green window includes the frequencies that can overlap. A and N indicate anomalous and normal dispersion, respectively. (d) Linear phase mismatch. The green solid curve points out the processes with group-velocity matching (see details in the text).

scenario represented in Fig. 3(d) with cascaded DW emission. In Fig. 5(c), we highlight the range of frequencies that could overlap due to GVD by means of a green background. SPM generates blue-shifted frequencies ($\omega > \omega_0$) at positive times and red-shifted frequencies ($\omega < \omega_0$) at negative times around the pulse center. As a result, blue-shifted frequencies that move faster, $\beta_1(\omega) < \beta_1(\omega_0)$, and red-shifted frequencies that move more slowly, $\beta_1(\omega) > \beta_1(\omega_0)$, will tend to get closer to each other [see Fig. 2(b)]. Among the potential interactions, those with suitable phase matching and group-velocity matching conditions will generate new frequencies more efficiently. Analogously to the first case studied in this section, FWM processes that satisfy both conditions [see Figs. 5(c) and 5(d)] yield spectral resonances observed in Fig. 5(a) for the green solid curve corresponding to a propagation distance of 7.5 mm (*i.e.*, the distance where $\mathcal{L}_{NL}^{-1}$ attains its first maximum). This physical explanation for the observed spectral resonances has not been presented before and provides new insights in the SC dynamics.

If the pulse propagates longer distances [see spectrum depicted by the blue dotted curve in Fig. 5(a)], additional processes can also take place, including the blue-shift in the resonance around 400 THz [19] and soliton fission. Since conservation of the initial pulse train structure is important for several practical applications, we have focused in this paper on spectral broadening mechanisms before pulse splitting [33]. Finally, we point out that, in addition to the cases studied here, we have verified that our framework also allows analyzing a wide panoply of other results reported in the literature [15, 19, 22, 23, 26, 42, 43].

5. Conclusions

Supercontinuum generation in integrated waveguides can be well-described by considering the third-order polarization that takes into account four-wave mixing, *i.e.*, $\omega_1 + \omega_2 \rightarrow \omega_3 + \omega_4$, and the frequency dispersion in the time domain. Therefore, any spectral change has to be related to these fundamental processes. Although dealing with complex nonlinear dynamics requires complete mathematical solutions of the nonlinear propagation equation — a high-level concept —, dominant four-wave mixing processes — low-level concepts — leading to dispersive wave emission, *i.e.*, spectral resonances, are identified in this work. Based on an analytically-solvable differential equation for the length scales where the nonlinearities and dispersion act at each propagation distance, we deconstruct the nonlinear pulse evolution and derive accurate analytical expressions for the high-order dispersion coefficients and the position of spectral resonances in several scenarios. Since low-level approaches does not make substantial differences between anomalous and normal dispersion regimes, our framework provides a unified description of dispersive wave emission in both normal and anomalous dispersion cases. The tables in the text compile the most important results.

Our tools are useful for nonlinear inverse engineering by setting a target dispersion curve providing the desired nonlinear response. Indeed, in this work we have designed the first octave-spanning supercontinuum source based on a foundry-compatible (220-nm-thick) silicon-on-insulator strip waveguide pumped at 1550 nm in the normal dispersion regime. In addition, our framework provides new physical insights about several reported experimental supercontinuum spectra in silicon and silicon nitride waveguides as well as optical fibers [15,19,21–23,26,42,43]. We believe our work strongly contributes to an in-depth comprehension, with an apparent practical purpose, of mechanisms to produce broadband light not relying on pulse splitting.

Funding

European Research Council (ERC-FP7/2007-2013 grant 336940); Vrije Universiteit Brussel (VUB-OZR); Federaal Wetenschapsbeleid (BELSPO-IAP); Flemish Government (Methusalem); Spanish Government, Ministerio de Economía y Competitividad (TEC 2013-46643-C2-1-R); Generalitat Valenciana (PROMETEO II/2014/072).

Appendix

In this appendix we draw the most important steps in the derivation of Eq. (4), Eq. (5) and the results included in Table 1. Let us consider the following properties for the generalized lengths that follow directly from Eq. (1) [36],

$$\mathcal{L}_{\mathrm{NL}}^{-1}(z) + \mathcal{L}_{\mathrm{D}}^{-1}(z) = \mathcal{L}_{\mathrm{NL}}^{-1}(0) + \mathcal{L}_{\mathrm{D}}^{-1}(0), \tag{7}$$

$$\frac{\mathrm{d}}{\mathrm{d}z}\mathcal{L}_{\mathrm{NL}}^{-1}(z) = -\beta_2\gamma_0 \frac{\int_{-\infty}^{\infty} \mathrm{d}t\, \partial_t\varphi(z,t)\partial_t|A(z,t)|^2|A(z,t)|^2}{\int_{-\infty}^{\infty} \mathrm{d}t\, |A(z,t)|^2}, \tag{8}$$

where φ is the phase of the complex envelope A. Let us consider that SPM initially governs the spectral broadening since $\mathcal{L}_{\mathrm{NL}}^{-1}(0) \gg \mathcal{L}_{\mathrm{D}}^{-1}(0)$. As a result, the chirp induced by GVD can be neglected at this stage and the most important effect of GVD is to broaden or compress the pulse in time. Based on these reasons, we assume $|A(z,t)|^2 = a(z)|A(0,a(z)t)|^2$ and $\varphi = b(z)\gamma_0|A(0,a(z)t)|^2$. Consequently, we neglect any pulse reshaping, similarly to the moment method [51], to evaluate the evolution of $\mathcal{L}_{\mathrm{NL}}^{-1}(z)$. However, unlike those methods, we are not looking for a detailed description of the pulse, but of $\mathcal{L}_{\mathrm{NL}}^{-1}(z)$. As a result, the approximation made is expected to be suitable even if the pulse is significantly distorted (*e.g.*, wave-breaking

regime). If these *ansatz* are introduced in the equations above and after performing some algebra, we derive the following equations:

$$\sigma_2\, a^2\, (\gamma_0 P_0 b)^2 \;=\; s_2\, N^2\, (1-a), \tag{9}$$

$$\frac{\mathrm{d}a}{\mathrm{d}\xi} \;=\; -2\, s_2\, \sigma_2\, (\gamma_0 P_0 b)\, a^3, \tag{10}$$

where $\sigma_2 = \int_{-\infty}^{\infty} \mathrm{d}\tau\ (\partial_\tau U)^2 U / \int_{-\infty}^{\infty} \mathrm{d}\tau\ U^2$, U being the peak normalized input pulse power [$|A(0,t)|^2 = P_0 U(t/T_0)$, where P_0 is the peak power and T_0 the duration of the input pulse], $\tau = t/T_0$, and N, s_2 and ξ have been defined in Section 2. If Eq. (9) is substituted in Eq. (10), then the next equation is derived:

$$\frac{\mathrm{d}a}{\mathrm{d}\xi} = -2\, s_2\, N\, a^2\, (s_2\, \sigma_2\ [1-a])^{1/2}\,, \tag{11}$$

that corresponds to Eq. (4) since $\mathcal{L}_{\mathrm{NL}}^{-1}(z) = a(z)\mathcal{L}_{\mathrm{NL}}^{-1}(0)$. This equation is trivially solved and provides the generalized wave-breaking distance, ξ_{GWB} [see Eq. (5) and Table 1].

Now we derive the spectral broadening induced by SPM. The maximum instantaneous frequency generated through SPM can be evaluated as $\delta\omega_{\mathrm{max}} = \max(-\partial_t \varphi) = -a(\gamma_0 P_0 b)\Upsilon T_0^{-1}$, where $\Upsilon = \max[\partial_\tau U]$. According to Eq. (9),

$$\delta\omega_{\mathrm{max}}(\xi) = \sigma_2^{-1/2} N\, (\, s_2[1-a(\xi)])^{1/2}\, \Upsilon T_0^{-1} \tag{12}$$

is obtained. Note that if $\delta\omega_{\mathrm{max}}$ is evaluated at ξ_{GWB}, then $\delta\omega_{\mathrm{GWB}}$ included in Table 1 is recovered.

Beyond ξ_{GWB}, the contribution of the GVD to the phase cannot be neglected (see Section 2). However, to calculate the values of β_3 and β_4 that induce DW emission, we need some estimates for $\xi > \xi_{\mathrm{GWB}}$. Following our reasoning in Section 2, we assume that the pulse at ξ_{GWB} can be described by a chirped Gaussian pulse, $A_{\mathrm{G}}(\xi_{\mathrm{GWB}}, t) = \exp\left(-(1+iC) a_{\mathrm{GWB}}^2 t^2 / 2T_0^2\right)$, where $a_{\mathrm{GWB}} = a(\xi_{\mathrm{GWB}})$. If we impose $\mathcal{L}_{\mathrm{D}}^{-1}(\xi_{\mathrm{GWB}}) = s_2 \mathcal{L}_{\mathrm{NL}}^{-1}(0)/2$ for such *ansatz*, then $C = N/a_{\mathrm{GWB}}\sqrt{2\tilde{\sigma}_2}$, regardless of s_2, where $\tilde{\sigma}_2 = \int_{-\infty}^{\infty} \mathrm{d}\tau\, \tau^2 |A_{\mathrm{G}}|^2 / \int_{-\infty}^{\infty} \mathrm{d}\tau\, |A_{\mathrm{G}}|^4$. The linear evolution of A_{G} beyond ξ_{GWB} (using the results in [38]) can capture the most relevant dispersive features of the pulse propagation in this second stage.

When $s_2 = -1$ (anomalous dispersion), Ref. [38] provides directly $a_{\mathrm{ol}} = (1+C^2)^{1/2} a_{\mathrm{GWB}}$, where $a_{\mathrm{ol}} = a(\xi_{\mathrm{ol}})$ is related to the pulse duration at the maximum compression distance, ξ_{ol}. In addition, if we still use Eq. (12) for $\xi_{\mathrm{ol}} > \xi_{\mathrm{GWB}}$, then we can obtain $\delta\omega_{\mathrm{ol}}$ appearing in Table 1.

On the opposite case, when $s_2 = 1$ (normal dispersion), we can also estimate the dispersive contribution to the chirp at the overlapping distance, $\delta\omega_{\mathrm{D,ol}}$, attending to [38], which provides directly $\delta\omega_{\mathrm{D,ol}} = a_{\mathrm{ol}}\xi_{\mathrm{ol}}(1+C^2)(\xi_{\mathrm{ol}} - \xi_{\mathrm{GWB}}) T_0^{-1}/\sqrt{2}$. Unlike the anomalous dispersion regime, it requires the knowledge of ξ_{ol}, which can be estimated through Eq. (11). Finally, if the definition $a_{\mathrm{ol}} = 1/4$ considered in this paper is used, then ξ_{ol} and $\delta\omega_{\mathrm{ol}}$ can be determined (see Table 1).

Acknowledgments

D. C.-L. thanks Prof. Magnus Karlsson for useful discussions.